A THREE-DIMENSIONAL MODEL OF LOW SPEED BLADE-VORTEX INTERACTION

BY

F. N. COTON, F. DE LA IGLESIA MORENO, R. A. McD. GALBRAITH, M. B. HORNER

UNIVERSITY OF GLASGOW
GLASGOW
G12 8QQ
SCOTLAND

TWENTIETH EUROPEAN ROTORCRAFT FORUM
OCTOBER 4 - 7, 1994 AMSTERDAM

A THREE-DIMENSIONAL MODEL OF LOW SPEED BLADE-VORTEX INTERACTION

F. N. Coton, F. de la Iglesia Moreno, R. A. McD. Galbraith, M. B. Horner

University of Glasgow
Glasgow
G12 8QQ
Scotland

1.   ABSTRACT

The development of a computational model to assist in the analysis of measurements from a wind tunnel study of low speed Blade-Vortex Interaction (BVI) is presented. In the technique, the wind tunnel test set-up is modelled by superposition of a three-dimensional free wake scheme with a two-dimensional vortex panel method and a convecting line vortex. Results from the model are used to confirm earlier deductions made on the basis of unsteady pressure measurements. Additionally, calculated velocity vectors in a plane perpendicular to the freestream direction are compared with Particle Image Velocimetry (PIV) images obtained during a parallel interaction. Finally, future enhancement of the technique is briefly discussed with particular reference to the unsteady response during BVI.

2.   NOMENCLATURE

c	blade chord length
C_n	normal force coefficient
r	radial position of measurement/calculation station
$\mathbf{r}$	position vector
r_c	vortex core radius
r_v	distance from vortex core
t	time
R	blade radius
V	velocity
X_v	horizontal distance between the leading edge, at the measurement position, and the vortex centre, measured perpendicular to the vortex core
Y_v	vertical displacement of the vortex generator junction above the rotor disk
Z_v	lateral displacement of the vortex generator from the tunnel centreline
δ	vortex generator section incidence
Γ	vortex circulation
$\bar{\Gamma}$	non-dimensional vortex circulation
Ψ	blade azimuth angle

3.   INTRODUCTION

Under certain conditions of powered descent or vigorous manoeuvring, rotorcraft blades pass through the wake and trailed tip vortices from previous blades. This interaction of the rotor blade with the tip vortex of a preceding blade has been identified as a significant source of noise and vibration in rotorcraft[1-3]. The need to reduce these undesirable effects requires that

the rotorcraft designer has a clear understanding of the fluid dynamics underlying the phenomenon of blade-vortex interaction. This need has been addressed through both experimental[4-20] and computational[21-24] studies attempting to isolate the BVI from the rotor environment.

In pioneering wind tunnel studies at the University of Pennsylvania, Surendraiah[4], and subsequently Padakannaya[5], utilised an upstream wing tip to generate a vortex that interacted with a downstream rotor. These studies were able to document many of the gross features of the blade-vortex interaction, including the development and collapse of a large leading edge suction peak, and the associated build up and reversal of the normal force. In studies[6-8] using a similar experimental technique, researchers working at NASA Ames were able to generate pressure data with better chordwise resolution than attained by Surendraiah and Padakannaya. In addition to the gross features of the interactions that had been previously identified, these researchers were able to document a "convective disturbance" in the aerofoil pressure distribution associated with the overhead passage of the interaction vortex. Unfortunately neither the study from the University of Pennsylvania nor the studies conducted at NASA Ames were able to provide flow field information, and therefore many of the important inferences associated with flow field behaviour remained unsubstantiated.

In studies at Glasgow, the effects of the passage of a vortex were examined in an experimental set-up similar to that developed by Surendraiah [25-28]. An upstream vortex generator was used to produce a vortex which interacted, either in parallel or oblique mode, with a downstream rotor set at zero blade incidence. The rotor blade was instrumented with 26 miniature pressure transducers which could be positioned at any one of five different spanwise locations. During the interaction process, these transducers were used to measure the evolution of chordwise pressure distribution and, by integration, the variations in force and moment coefficients. This work was further enhanced by a series of flow visualisation tests, conducted in collaboration with Heriot-Watt University, in which Particle Image Velocimetry (PIV)was used to obtain high quality images of the local blade flow field at various stages of the interaction process [29-30].

The present study concentrates on the development of a computational model to assist in the analysis of the collected data and to provide additional insight into the convective properties of the vortex during interaction. It was intended that the model would be conceptually simple but, nonetheless, comprehensive and that it would be used to reproduce a variety of interaction scenarios. BVI modelling has been the focus of considerable attention, particularly since the early nineteen eighties. Since then, a variety of different modelling techniques have been applied to the BVI problem although many of these are not readily adaptable to a fully three-dimensional environment. The model developed in the present study utilises the principle of superposition to combine basic features of the 3-D interaction and has evolved from an earlier scheme which originated as a student project [31].

In the computational model, the wake from the experimental rotor is represented by a lattice of shed and trailed vorticity elements which are free to convect under the influence of the free stream and induced velocity components. The strengths of the trailed and shed vorticity filaments are determined from the spanwise and azimuthal load variations on the rotor blade which is modelled as a series of bound vortex segments. To reproduce the BVI, the rotor model is combined with a convecting vortex which is represented as a continuous series of equal strength vortex filaments which, like the wake model, are free to convect. At each spanwise location on the blade, a 2-D vortex panel method is used to evaluate the local circulation and chordwise pressure distribution. This panel method also includes a cross-sectional representation of the convecting vortex and so modifies the chordwise pressure distribution accordingly. Thus, at each spanwise blade section, the free stream and wake induced velocities define the effective angle of attack which is, in turn, input to the modified

panel method. This hybrid model is also combined with an algorithm which allows calculated velocity vectors in any plane perpendicular to the free stream direction to be visualised. This facility is included to permit direct comparison with the experimentally obtained PIV images.

In this paper, the model is used to look at a variety of Blade Vortex Interactions. Initially, the stability of the technique is demonstrated by consideration of a head-on perpendicular interaction between a fixed vortex and a rectangular wing. The physical configuration of the Glasgow University BVI test facility is then modelled for both the oblique and parallel interaction of a convecting vortex with a rotating blade. Results for the oblique case are shown to confirm the existence and behaviour of an 'intersection vortex' which, it had been postulated, accounts for many of the differences between oblique and parallel BVI's. The model is then used to consider the parallel interaction case and is compared with a series of Particle Image Velocimetry measurements made during a close interaction.

4.   MODEL FORMULATION

For most of the cases presented in this study, the BVI model is configured to represent the experimental facility at Glasgow University. A schematic of this facility is shown in Fig. 1.

4.1   Rotor model

The rotor blade is modelled as a series of bound vortex segments which are located along the quarter chord line of the blade. As the blade rotates and comes under the influence of the interacting vortex, the spanwise and azimuthal variations in this bound vorticity distribution require vorticity to be trailed and shed from the blade. In the model, this process is discretized to produce an evolving lattice of finite length vortex filaments in the wake of the blade, as shown in Fig. 2. Thus, at each time step, trailed vortex filaments corresponding to the spanwise variation in blade bound vorticity are added to the wake lattice. Similarly, shed filaments, whose strengths are determined by the temporal change in bound vorticity at each radial location, are also added to the wake. The manner in which these filaments move as part of the wake structure is then determined by a free wake approach in which the wake shape is modified at each time step according to the velocities induced at the lattice nodes. The total induced velocity at any node is calculated by application of the Biot-Savart equation between that node and all wake filaments and bound vorticity elements on the blade. Once the induced velocity at a given node is known, its positional change is determined by integration of the velocity field according to the second order Adams-Bashforth equation.

$$\bar{r}(t + \Delta t) = \bar{r}(t) + \left[\frac{3}{2} \bar{V}(t, \bar{r}(t)) - \frac{1}{2} \bar{V}(t - \Delta t, \bar{r}(t - \Delta t)) \right]$$ (1)

In the rotor model there is no wake behind the blade at the first time step and, consequently, classical lifting line theory is applied to estimate the induced velocity and, hence, loading distribution on the blade. At all subsequent time-steps, however, the wake structure is represented by the lattice of shed and trailed vortex filaments described above and so an alternative method is applied to determine the blade loading distribution.

As the blade moves to a new position, vortex filaments are added to the wake lattice in the manner described above. The strengths of these filaments depend on the unknown distribution of bound vorticity at the new blade position and so must be determined as part of the solution. In the present method, the strengths of the filaments are initially set at the corresponding values for the previous time-step. This allows a first estimate of the induced velocity distribution at

the blade to be made and, from this, an initial bound vorticity distribution to be calculated. Once this has been done, the strengths of the vortex filaments are then updated and a new estimate of the blade loading distribution is made. This procedure is repeated until a converged solution is obtained.

The requirement to predict chordwise pressure distributions at each spanwise location on the rotor blade is not fulfilled by the basic rotor model described above. For this reason, and to avoid the complexity of a fully three-dimensional surface representation, a two-dimensional vortex panel method was embedded within the rotor model. This panel method is used, in conjunction with the induced velocity predicted by the free wake model, to evaluate the local circulation and chordwise pressure distribution at each spanwise station on the blade. The output from the panel method thus determines the strength of the bound vorticity at a given spanwise location. A schematic of this form of blade model is shown in Fig. 3.

4.2   Blade Vortex Interaction Model

The basic methodology adopted for the BVI simulation involves the superposition of a convecting line vortex with the rotor model. In the method, the vortex is represented by a connected series of finite length, constant strength filaments which travel with the free stream. As these filaments come under the influence of the rotor system, their path is altered by the induced flow field. The manner in which this occurs is determined by the same technique as that applied to the rotor wake.

In a model of this type, it is essential that the influence of each flow element is fully represented in the computational algorithm. For any given filament in the convecting vortex set, the effects of all other flow elements simply take the form of contributions to the total induced velocity calculated at that filament. The technique used to include the effect which the convecting vortex has on the rotor system is, however, more subtle and requires careful consideration.

As indicated previously, the rotor wake convects according its induced velocity field. In this regard, it behaves in the same way as the convecting vortex set. Consequently, the same technique used to calculate the effect of the rotor system on the convecting vortex can be used to evaluate the effect which the convecting vortex has on the rotor wake. The influence of the vortex on the rotor blade, however, cannot be adequately represented in this way and so a different technique is applied. This involves incorporation of the convecting vortex within the two-dimensional vortex panel method solution at each spanwise station. The first step in this process is the determination of a two-dimensional representation of the convecting vortex at its point of intersection with the plane at which each spanwise calculation is carried out. It should be noted that, if a finite angle exists between the rotor blade and the convecting vortex, an elongated two-dimensional form of the basic vortex will result. Superposition of the vortex within the panel method is achieved by addition of the induced normal velocity component due to the vortex at each panel control point. Thus, when the panel method solution is calculated, the boundary condition of zero normal velocity on the surface produces a modified velocity distribution which includes the direct effect of the vortex. The strength of the corresponding bound vorticity can then be calculated for subsequent use in the rotor model.

4.3   Root Cut-off

To eliminate the development of any numerical instabilities caused by the rotor hub arrangement, it was necessary to introduce a root cut-off at 20% of the rotor radius. This portion of the blade experiences a very low dynamic pressure and, in the experiment, is almost

entirely taken up by the rotor hub. Consequently, it contributes little to the blade aerodynamic behaviour.

4.4   Vortex Core Correction

Several vortex core models were considered for the present work. Of these, a Scully representation was adopted in the form of a correction factor

$$\frac{r_v^2}{\left(r_v^2 + r_c^2\right)} \tag{2}$$

applied to the induced velocity calculation. The core radius was taken to be approximately 17% of the blade chord which is consistent with PIV measurements on the experimental rig.

5.   EXPERIMENTAL METHODS

5.1   Blade Vortex Interaction Facility

Experiments were conducted in the University of Glasgow Handley Page wind tunnel in collaboration with the PIV facilities of Heriot-Watt University. An untwisted, non-lifting, single blade rotor interacted in a parallel or oblique manner with an oncoming vortex generated upstream of the rotor disk by a stationary wing. This set-up is depicted in Fig. 4.

The aluminium rotor blade had a NACA 0015 aerofoil section, with a 0.149 m chord and a 0.9426 m radius. The vortex generator consisted of two adjoining NACA 0015 aerofoil sections spanning the height of the test section 2.1 rotor radii upstream of the rotor hub. During the test sequence conducted in the 1.61 x 2.13 m octagonal test section, the tunnel speed was 47.0 m/s while that of the rotor tip was 59.25 m/s. The vortex strength was controlled by setting the two sections of the vortex generator at equal but opposite incidence. The horizontal position of the vortex generator (Z_v) was altered to control the angle of intersection between the interaction vortex and the blade, resulting in either a nominally parallel or oblique BVI. The vertical position of the aerofoil junction on the vortex generator (Y_v) was varied to allow an examination of interactions for different blade-vortex separation heights.

5.2   Unsteady Pressure Measurement

An instrumented pod containing 26 miniature pressure transducers (3 KULITE XCS-093-5-SG transducers and 23 ENTRAN-EPIL-080B-5S transducers) could be located at one of five spanwise positions on the blade. The 26 transducer voltages were amplified, low pass filtered, then simultaneously digitised by a Thorn EMI BE256-420 data logger before being stored in an IBM PS/2 80/041 computer for further reduction and presentation. Data collection was phase locked to azimuth position and each test run comprised the collection of data during many (typically 7) interactions. Data were subsequently ensemble averaged about the C_n cross over point; the point near $X_v/C=0.0$, where the normal force drops through zero, between the peak and nadir in C_n. Pressure data were integrated around the aerofoil section to provide force and moment data. Pressure, force and moment data were non-dimensionalised into aerodynamic coefficients using the local chordwise velocity at the measurement location when the blade was at the 180° azimuthal position.

5.3   Particle Image Velocimetry

PIV data were collected in one of two planes oriented perpendicularly to the tunnel free stream, one plane at 0.78 rotor radii upstream of the rotor hub, and the second at 0.94 rotor radii.

Particle Image Velocimetry data were collected in the measurement plane by photographing the seeding particles, illuminated by a pulsed sheet of laser light. A 35 mm camera (Nikon F801) was mounted below the rotor hub, facing upstream. Images were collected on Kodak Recording Film 2475 using a 55 mm flat field lens. The camera mount was constructed of 49 mm box section mild steel, attached directly to the floor of the wind tunnel bay, thus isolated from the vibration of the tunnel and rotor system. A faring covering the camera mount and the lower half of the rotor shaft was also employed to shield the camera mount from any aerodynamic buffeting. An accelerometer attached to the top of the camera mount indicated that errors in velocity measurement due to camera vibration were less than 0.3% of full span.

The laser light required was provided by a Lumonics HLS4 ruby laser. The laser beam was formed into a light sheet using a simple lens configuration. Triple pulses of laser light were used to generate multiple images of each seed particle on the photographic film, thus allowing later calculation of local velocities in the vicinity of each particle. Laser pulses were typically separated by 50 to 100 μs, with each individual pulse having an energy of approximately 1.5 J. Directional ambiguity was addressed in a select number of tests by setting the first inter-pulse interval longer than the second. This procedure results in unequally spaced 3 spot patterns which can be used to derive flow direction. Most tests, however, utilised constant inter-pulse intervals of 60 to 80 μs.

Image processing was carried out in the Fluid Loading and Instrumentation Centre in the Department of Offshore and Civil Engineering at Heriot-Watt University in Edinburgh. During image processing the negatives are mounted on an X-Y traverser and interrogated using a CCD camera and microscope lens arrangement. Each 35 mm negative is subdivided into 80 frames (512 x 512 pixels) which are individually digitised. Computer software is then employed to automatically identify particle pairs or triples, and determine local velocity. A manual check is required for the rejection of spurious velocity vectors. Image processing requires approximately 1-2 hours, as a result conventional data averaging is excessively time consuming and was not used.

To obtain a reasonable sequencing of the images 12 or more images were recorded of each azimuthal position and relative positions of the blade and vortex in each of the twelve images were then determined. A judicial selection was then made and the chosen frame processed. Under some conditions the interaction vortex passes above the aerofoil and so out of the camera's view. In these cases a second camera, mounted above the rotor hub, and operating simultaneously with the lower camera, was used. Data from the upper camera simply documented the overhead position of the vortex as an aid in selecting the lower camera image representative of flows beneath the blade. The upper camera was not used for collecting velocimetry data.

6. RESULTS AND DISCUSSION

6.1 Perpendicular Blade Vortex Interaction

The axisymmetric loading produced by the perpendicular interaction of a fixed vortex with a rectangular planform wing provided a suitable test for the stability of the numerical method. The particular case studied was that of a rectangular blade at zero incidence at a fixed azimuth of 90° interacting with a fixed vortex of strength $\Gamma=10m^2/s$. The vortex was positioned at the mid-span of the wing.

The evolution of the vortex wake for this case is shown in Figs. 5a-5c. In the first figure (t=0.011s), the wake begins to wrap around the interaction vortex. As may be expected, the strongest trailed vorticity in the wake (indicated by line thickness) is confined to the vicinity of the interaction vortex. At the end of the wake there is a strong shed vortex system associated with the calculation start-up condition. Conversely, there is almost no evidence of shed vorticity near the trailing edge of the blade indicating that the calculation is already approaching the steady state condition. There is some loss of symmetry at the end of the wake.

In Figs. 5b and 5c. the instability near the start-up system continues to develop as the wake progresses downstream. Nonetheless, there is no evidence of this instability moving upstream towards the blade and, indeed, the calculation converges towards a stable solution.

6.2 Oblique Blade Vortex Interaction

In an earlier study by Horner et al. [27], the effects of the intersection angle during an oblique BVI were considered. As shown in Fig. 6, it was found that, during second quadrant BVIs (where the blade is advancing in the clockwise sense and interacting with a vortex positioned to the left of the rotor hub), C_n values recorded on outboard sections of the blade were initially greater than those of equivalent parallel interaction cases; i.e. with the same non-dimensional vortex strength. As the vortex moved closer to the measuring section, however, the magnitudes of the parallel C_n data increased more rapidly than the oblique data, eventually reaching a higher and sharper peak. The load reversal was also more abrupt in the parallel case. Data recorded after the vortex had passed the aerofoil leading edge showed a much higher level of agreement between the two cases.

The behaviour witnessed in the above study was attributed to two specific effects. During the approach to the oblique BVI, the measurement position is closer to the interacting vortex than the blade tip; unlike the parallel case where the two are almost equidistant. Consequently, a comparatively weaker tip vortex is produced in the oblique case and the corresponding incidence reduction effected by the vortex is less than under parallel interaction conditions. Thus, higher C_n values are observed in the early part of the C_n history.

It was postulated that another significant influence on the measured interaction data was the vorticity trailed from the blade at the point where it intersects with the oncoming vortex. This vorticity, termed the 'intersection vortex', would act in such a way as to reduce the effective incidence of outboard blade sections. Thus, it may be expected that, as this intersection vortex moves close the measuring section, there may be a reduction in measured normal force. It was considered likely, however, that, in the oblique case studied, the duration of any significant effect would be very short because of the rapid rate at which the intersection vortex approaches the measuring section. This may explain the reduction in magnitude of the peak in the C_n curve measured in the oblique case.

The model developed in this study has been used to investigate the existence of the intersection vortex by modelling a similar oblique interaction to that examined above. Of particular interest in this study was the manner in which the intersection vortex was manifest and what, if any, influence it had on the structure of the wake trailed from the blade. The actual test configuration modelled was that of a second-quadrant oblique interaction ($\Gamma=6.7m^2/s$) with the vortex generator offset from the rotor hub by two chord lengths to the left.

Figure 7a, shows the vortex wake trailed behind the blade at azimuth 138°. It should be noted here that the calculation was initiated at 90° azimuth; hence the relatively short wake. In the diagram, vortex strength is indicated by line thickness with no line being plotted for very weak filaments. It is clear that a strong vortex, of approximately half the strength of the interaction vortex, is trailed from the intersection point on the blade. This vortex is, at this stage clearly stronger than the tip vortex. Additionally, the shape of the vortex within the wake structure is closely related to the history of the movement of the intersection point position. There is very little evidence of any wake roll-up in the vicinity of the intersection vortex except at the far end of the wake where the start-up system is significant. Further examination of the wake structure from a 3-D perspective (Fig. 7b), however, shows a more substantial local deformation of the wake in the vicinity of the intersection vortex. This deformation, with no apparent roll-up, is consistent with that which would be produced by two strong vortices of opposite sign. It is possible, that the near balance of the two prevents roll-up of the wake around the trailed intersection vortex.

In Fig. 8, the blade has advanced to an azimuth of 150°. Again the intersection effect is clearly visible although, in this case, the intersection is moving outboard more rapidly and is spread over more of the span. Consequently, the intersection vortex is less well defined and, in the model, is not readily identifiable as a single trailed vortex. The deformation in the wake structure is also noticeably reduced in the vicinity of the blade. Nonetheless, the trailed vorticity emanating from the intersection region is still of equivalent magnitude to the tip vortex.

From the figures presented above, the formation and progression of the so-called intersection vortex may be clearly observed. Initially, the vortex is very strong but apparently reduces in strength as the azimuth angle of the blade is increased. The behaviour documented here is akin to that postulated by Horner et al. but further detailed examination of spanwise loading histories will be necessary to fully characterise the detailed role of the intersection vortex.

6.3   Parallel Blade Vortex Interaction

Use has been made of the present model to predict azimuthal load variations due to a parallel BVI where the vortex is positioned approximately one chord length above the aerofoil. In Fig. 9, the predicted C_n history due to a vortex of strength 3.4m²/s, is compared to equivalent wind tunnel data. Of immediate concern is the disparity in the magnitude and location of peak C_n. This may be partially explained by the observed [29] wander of the vortex during the wind tunnel tests, although it would be expected that the data averaging process should account for this effect. A more likely reason for the difference in the position of peak C_n and the subsequent slope of the C_n curve could be a slight error in the predicted convection of the interaction vortex. This would not be surprising given that the calculation does not include either the tunnel walls or the rotor hub. The difference in the magnitude of peak C_n may be due the uncertainty associated with the strength of the experimental vortex. This was first highlighted

in an earlier study [29], which compared the velocity distribution measured across a vortex using PIV with the vortex strength obtained via a triple hot wire.

The calculation described above was not conducted at sufficiently high resolution to allow examination of the tangential or pitching moment histories. Nevertheless, the general form of the predicted C_n variation warrants further work in this area.

As part of the present work, an algorithm was developed which allows calculated velocity vectors in any plane perpendicular to the free stream direction to be visualised. This facility enables a direct comparison with experimentally obtained PIV images to be made.

In Figs. 10-12, a series of PIV images are compared with calculations for the parallel interaction case at the 78% span location for a vortex of strength $6.7 m^2/s$ positioned 0.2 chord lengths below the blade. In Fig. 10, azimuth angle 168°, the vortex is approaching the leading edge of the blade. Both images exhibit the same general feature of substantial upwash at the blade leading edge. Similarly, the arched appearance of the flow on the upper surface of the blade is well modelled.

In Fig. 11, the blade has moved on to an azimuth of 176°. Here, the vortex is positioned just below the leading edge of the aerofoil in the PIV image but is nearer to the quarter chord location in the calculated flow field. At this point, the rate of change of normal force coefficient is extremely high, according to measured pressure data. Consequently, the local flow in the vicinity of the aerofoil will have a significant dynamic component which is, as yet, not represented in the current quasi-steady model. Considering this, together with the deficiencies of the physical model described above, it is not surprising that some discrepancy in the vortex position is apparent at this stage.

The flow patterns associated with a blade azimuth of 191° (193° experimental) are presented in Fig 12. Again, the general form of the measured flow field is well represented by the calculation. In particular, the deformation of the interaction vortex as it moves into the shed vortex system behind the aerofoil is noticeable. In both figures, there is clearly a vortical structure to the left of the interaction vortex. From the PIV images alone it was unclear whether this structure was due to an earlier shed vortex or to the tip vortex moving into the measurement plane. Using the model, however, it was possible to establish that the tip vortex was responsible for the observed structure.

7.   CONCLUDING REMARKS

The model presented in this study is at an early stage of development. To date, the model has been used to examine specific phenomena associated with an experimental test programme. In this respect, it has provided useful information to substantiate behaviour inferred from earlier observations. The next stage in the model development will involve comprehensive validation of the technique against the extensive database of unsteady pressure and PIV measurements available at Glasgow University. In the validation process, it is hoped to identify the limits of the current modelling philosophy. Beyond this, the extension of the model to the unsteady case will be considered. It is hoped that, in view of the highly localised nature of the BVI phenomena, it may be possible to introduce a zonal treatment of the flow, thus reducing computation time. It may also be possible to introduce the effects of viscosity in a similar manner.

8. ACKNOWLEDGEMENTS

9. REFERENCES

1) Scheiman, J. and Ludi, L.H., "Qualitative Evaluation of Effect of Helicopter Rotor-Blade Tip Vortex on Blade Airloads" NASA TN D-1637, May, 1963.

2) Brotherhood, P., and Riley, M.J., "Flight Experiments on Aerodynamic Features Affecting Helicopter Blade Design", Vertica, Vol. 2 , pp. 27-42, 1978.

3) Schmitz, F.H., Boxwell, D.A., Lewy, S., and Dahan, C., "Model- to Full-Scale Comparisons of Helicopter Blade-Vortex Interaction Noise", 38th Annual National Forum of the American Helicopter Society, Anaheim, Calif., May, 1978.

4) Surendraiah, M. "An Experimental Study of Rotor Blade-Vortex Interaction", M.S. Thesis, The Pennsylvania State University, December, 1969.

5) Padakannaya, R. "Experimental Study of Rotor Unsteady Airloads due to Blade Vortex Interaction", NASA CR - 1909, November, 1971.

6) Caradonna, F.X., Laub, G.H. and Tung, C. "An Experimental Study of Rotor-Vortex Interaction", NASA TM-86005, November, 1984.

7) Caradonna, F.X., Lautenschlager, J.L. and Silva, M.J., "An Experimental Study of Rotor-Vortex Interactions", AIAA Paper 88-0045, AIAA 26th Aerospace Sciences Meeting, Reno, Nevada, January, 1988.

8) Caradonna, F.X., Strawn, R.C., and Bridgeman, J.O.,"An Experimental and Computational Study of Rotor-Vortex Interactions", 14th European Rotorcraft and Powered Lift Aircraft Forum, Milano, Italy, September, 1988.

9) Seath, D.D. "Vortex-Airfoil Interaction Tests", 2nd Atmospheric Flight Mechanics Conference, Palo Alto and Moffett Field, California, September, 1972.

10) Seath, D.D., Kim, J.M. and Wilson, D.R. "An investigation of the Parallel Blade-Vortex Interaction in Low-Speed Wind Tunnel", AIAA Paper 87-1345, AIAA 19th Fluid Dynamics, Plasma Dynamics and Lasers Conference, Honolulu, Hawaii, June, 1987.

11) Ham, N.D. "Some Preliminary Results from an Investigation of Blade-Vortex Interactions", Journal of the American Helicopter Society, Vol. 19, pp. 45-48, April, 1974.

12) Ham, N.D. "Some Conclusions from an Investigation on Blade-Vortex Interaction", Journal of the American Helicopter Society, Vol. 20, pp 26-31, October, 1975.

13) Booth, E.R. Jr. and Yu, J.C. "Two-Dimensional Blade-Vortex Flow Visualisation Investigation", AIAA Journal Vol. 24, No. 9, September, 1986.

14) Booth, E.R. Jr. "Surface pressure Measurement During Low Speed Two-Dimensional Blade Vortex Interaction", AIAA Paper 86-1856, AIAA 10th Aeroacoustics Conference, Seattle, Washington, July, 1986.

15) Meier, G.E.A. and Timm, R."Unsteady Vortex Airfoil Interaction" AGARD CP - 386, May, 1985.

16) Straus, J., Renzoni, O. and Mayle, R.E. "Airfoil Pressure Measurements During a Blade-Vortex Interaction and a Comparison with Theory", AIAA Paper 88-0669, AIAA 26th Aerospace Sciences Meeting, Reno, Nevada, January, 1988.

17) Huyer, S. A., and Luttges, M. W. "Unsteady Flow Interactions Between the Wake of an Oscillating Airfoil and a Stationary Trailing Airfoil", AIAA Paper 88-2581, AIAA 6th Applied Aerodynamics Conference, Williamsburg, Virginia, June 1988.

18) Ziada, S. and Rockwell, D. "Vortex-Leading Edge Interaction", Journal of Fluid Mechanics, Vol. 118, pp. 79-107, 1982

19) Walker, J. "Dynamic Stall Wake Interaction with a Trailing Aerofoil", AIAA Paper 87-0239, AIAA 25th Aerospace Sciences Meeting, Reno, Nevada, Jan. 1987

20) Sears, W.R. "Aerodynamics, Noise and the Sonic Boom", AIAA Journal, Vol. 7, No. 4, April, 1969.

21) Panaras, A. "Numerical Modelling of the Vortex-Airfoil Interaction", AIAA Journal, Vol. 25, No. 1, January, 1987.

22) Lee, D.J. and Smith, C.A. "Distortion of Vortex Core during Blade/Vortex Interaction", AIAA Paper 87-1243, <u>AIAA 19th. Fluid Dynamics,</u> Plasma Dynamics & Lasers Conference Honolulu, Hawaii, June, 1987.

23) Jones, H.E., and Caradonna, F.X., "Full Potential Modelling of Blade-Vortex Interactions", <u>Vertica Vol. 12 No. 1/2,</u> pp. 129-145, 1988.

24) Visingardi, A., "A Boundary Integral Formulation for the Aerodynamic Analysis of Parallel Blade-Vortex Interactions Over Aerofoils", <u>19th European Rotorcraft Forum,</u> Como, Italy, 1993

25) Kokkalis, A. and Galbraith, R.A.McD. "Results from the Glasgow University Blade-Vortex Interaction Facility", <u>13th European Rotorcraft and Powered Lift Aircraft Forum,</u> Arles, France, September, 1987.

26) Horner, M.H., Saliveros, E., Kokkalis, A., and Galbraith, R.A.McD., "Results from a Set of Low Speed Blade-Vortex Interaction Experiments", Glasgow University Aero Report 9109, July, 1991. To be published in Journal of Experiments in Fluids

27) Horner, M.H., Saliveros, E., and Galbraith, R.A.McD., "An Experimental Investigation of the Oblique Blade-Vortex Interaction", <u>17th European Rotorcraft and Powered Lift Aircraft Forum,</u> Berlin, Germany, September, 1991.

28) Horner, M.H., Saliveros, E., and Galbraith, R.A.McD., "An Examination of Vortex Convection Effects During Blade-Vortex Interaction", <u>AHS/RAeS Technical Specialists Meeting on Rotorcraft Acoustics and Rotor Fluid Dynamics,</u> Philadelphia, U.S.A., October, 1991.

29) Horner, M.H., Stewart, J.N., Galbraith, R.A.McD., Grant, I., Coton, F.N., Smith, G.H., "Preliminary Results from a Particle Image Velocimetry Study of Blade Vortex Interaction", <u>19th European Rotorcraft Forum,</u> Como, Italy, 1993

30) Horner, M.H., Stewart, J.N., Galbraith, R.A.McD., Grant, I., Coton, F.N.,"An Examination of Vortex Deformation During Blade-Vortex Interaction Utilising Particle Image Velocimetry", <u>19th Congress of the International Council of Aerospace Sciences,</u> Anaheim, California, USA, 1994

31) De la Iglesia, F, "Development of a Fully Unsteady Blade-Vortex Interaction Model", Dept of Aerospace Engineering, University of Glasgow, 1993
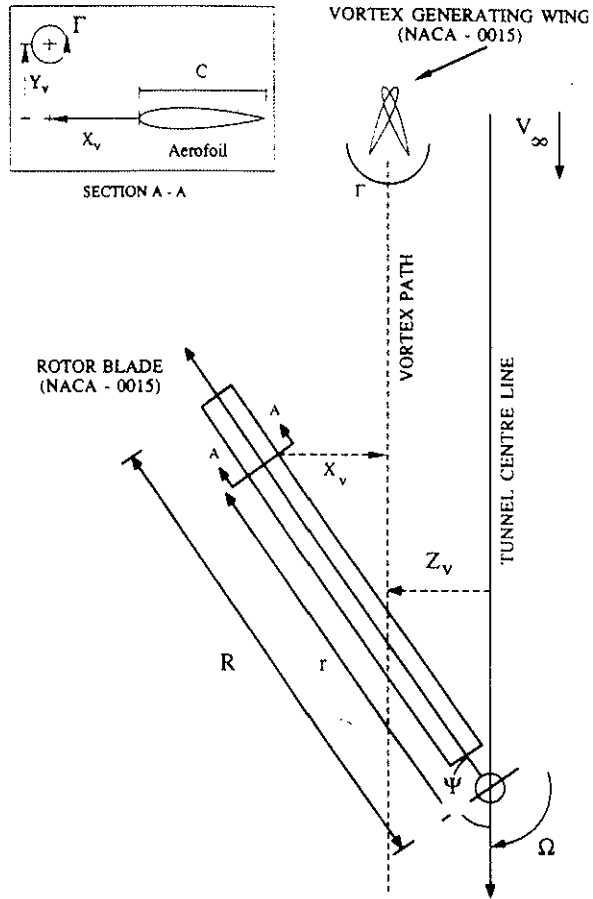
Figure 1.   Schematic of Glasgow University BVI facility
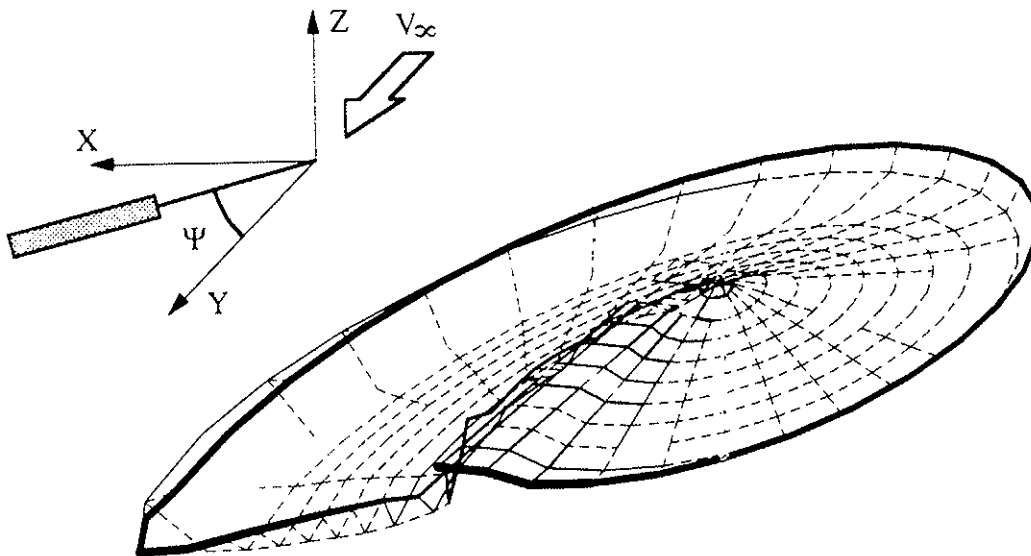
Figure 2.   Typical wake lattice generated by rotor code

Aerofoil panel distribution.

Bound Vortices

Γ_4 Γ_5 Γ_6 Γ_7

Γ_3

Γ_2

Γ_1

$-\Gamma_7$

$\Gamma_7-\Gamma_6$

$\Gamma_6-\Gamma_5$

$\Gamma_5-\Gamma_4$

$\Gamma_4-\Gamma_3$

$\Gamma_3-\Gamma_2$

$\Gamma_2-\Gamma_1$

Γ_1

Blade represented as
a lifting line

Trailing Vortices
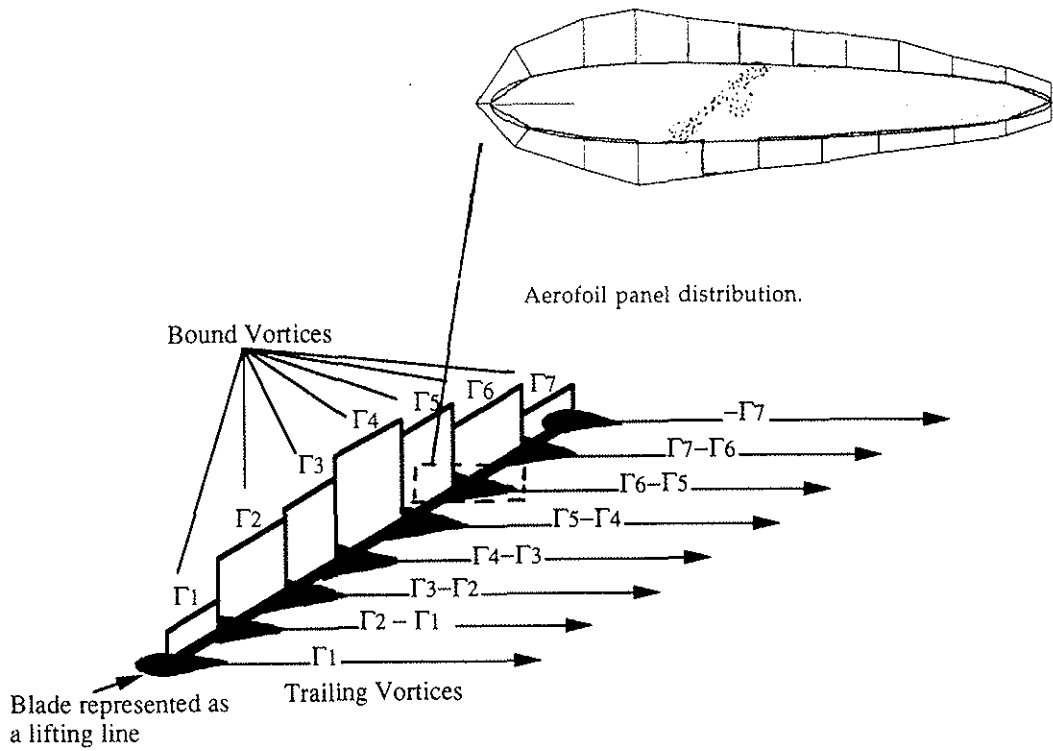
Figure 3.   Schematic of rotor blade model
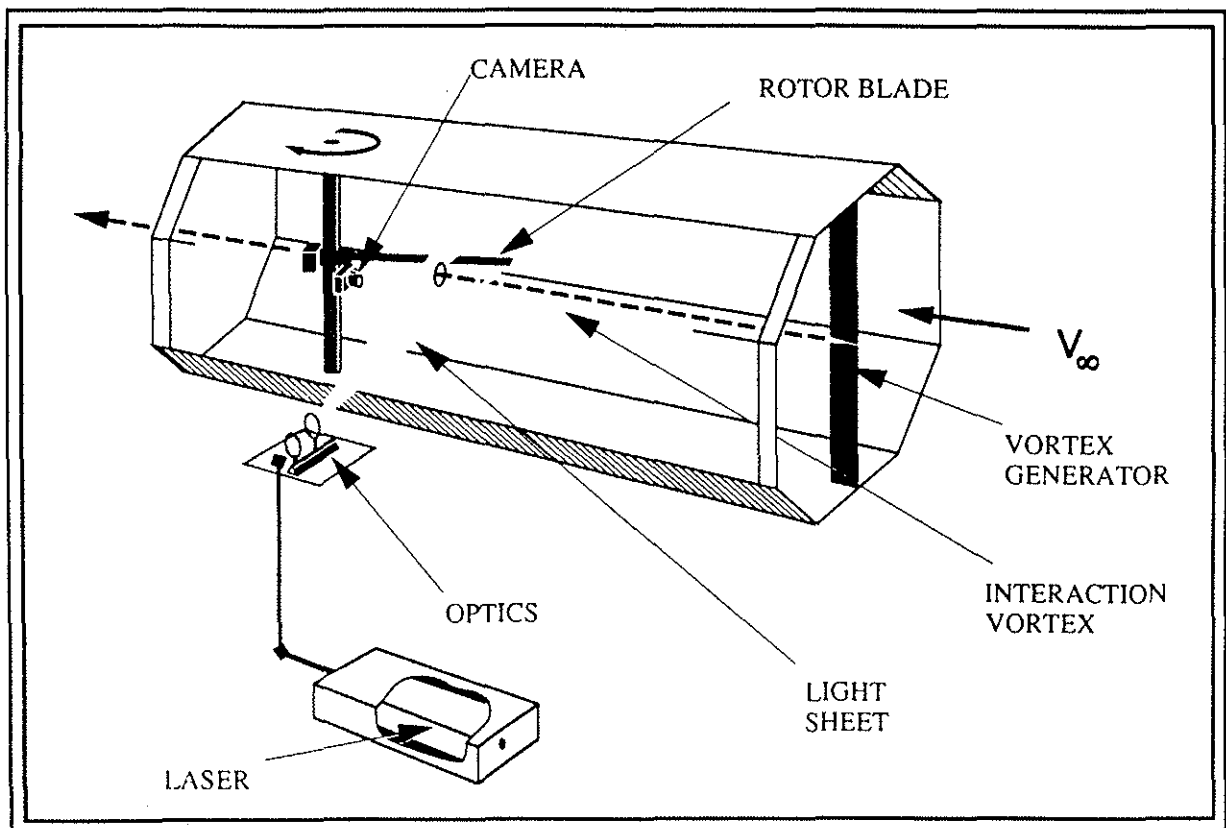
Figure 4.   Set-up of the Glasgow University BVI facility

18-13

(a) t = 0.011s

(b) t = 0.019s

(c) t = 0.026s
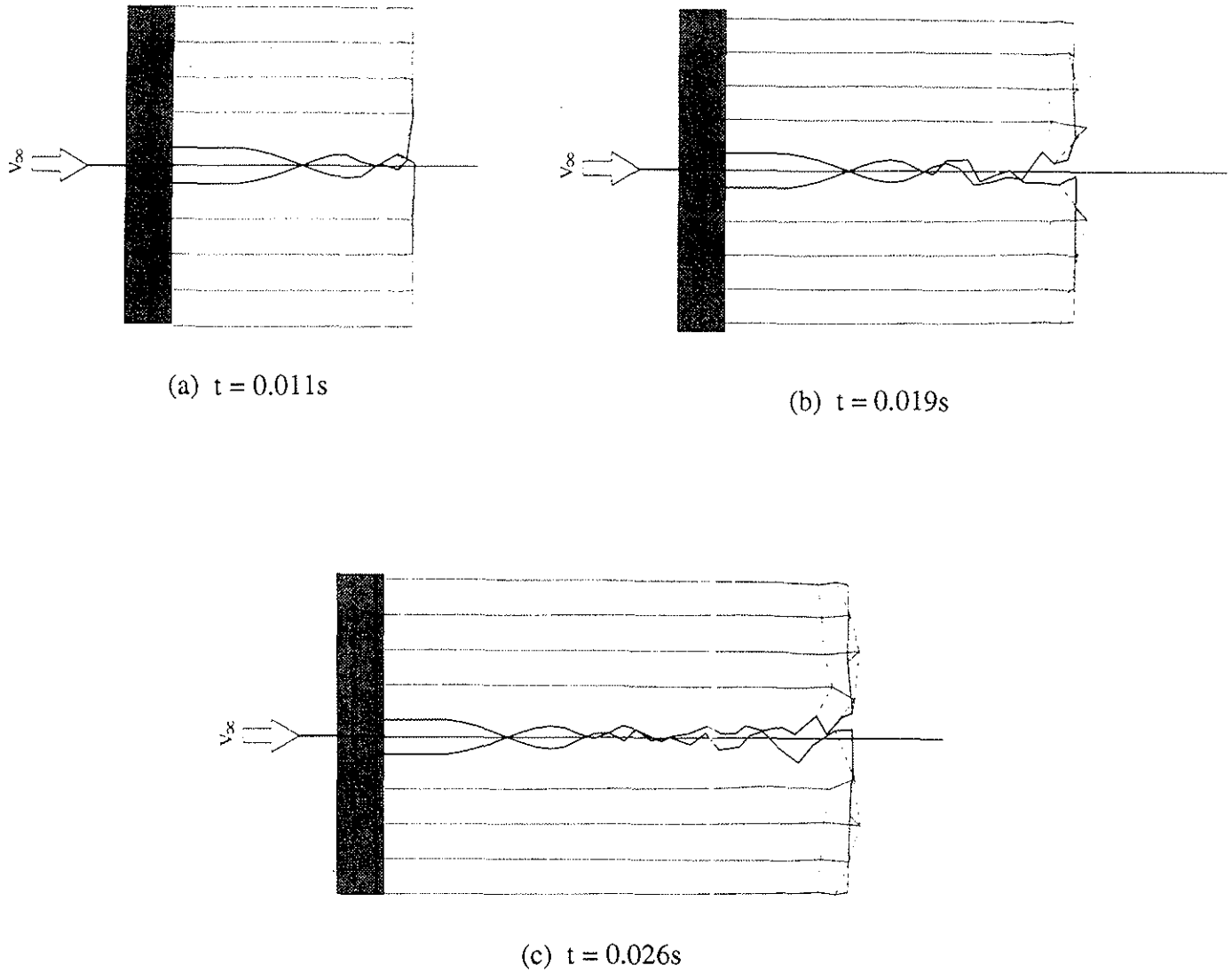
Figure 5.   Temporal development of the wake geometry due to a perpendicular interaction with a fixed vortex.
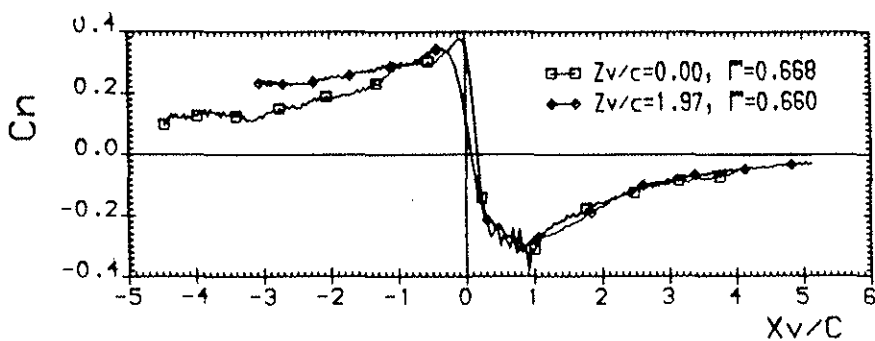
Figure 6.   A comparison of integrated C_n data for comparable parallel and second quadrant oblique interactions. (r/R =0.865, Y_v/c=0.2)
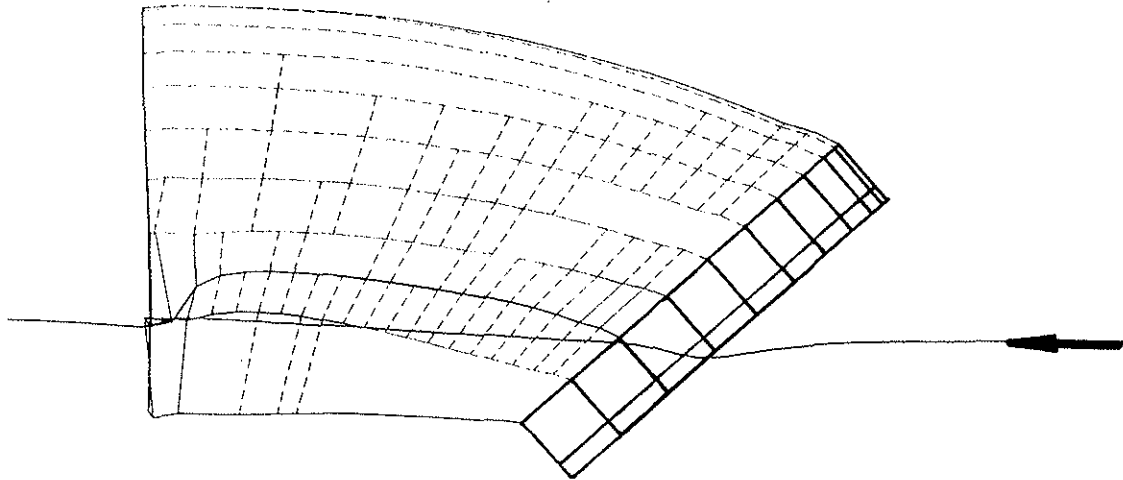
(a) two-dimensional view
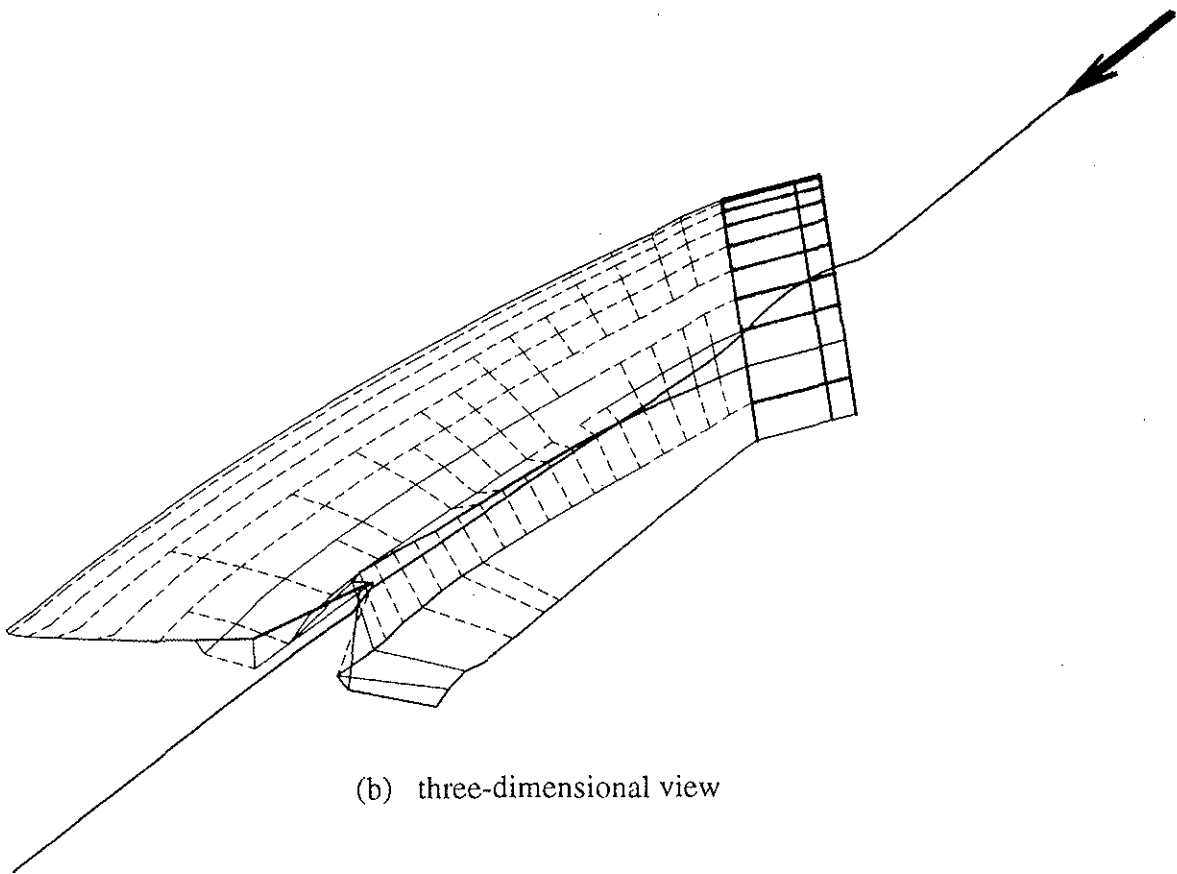
(b) three-dimensional view

Figure 7.   Calculated wake shape at $\Psi =138°$ during a second quadrant oblique interaction where $\Gamma = 6.7 m^2/s$, $Z_v/c =2$ and $Y_v/c=0.2$. (Line thickness indicates vortex strength in the wake)

18-15
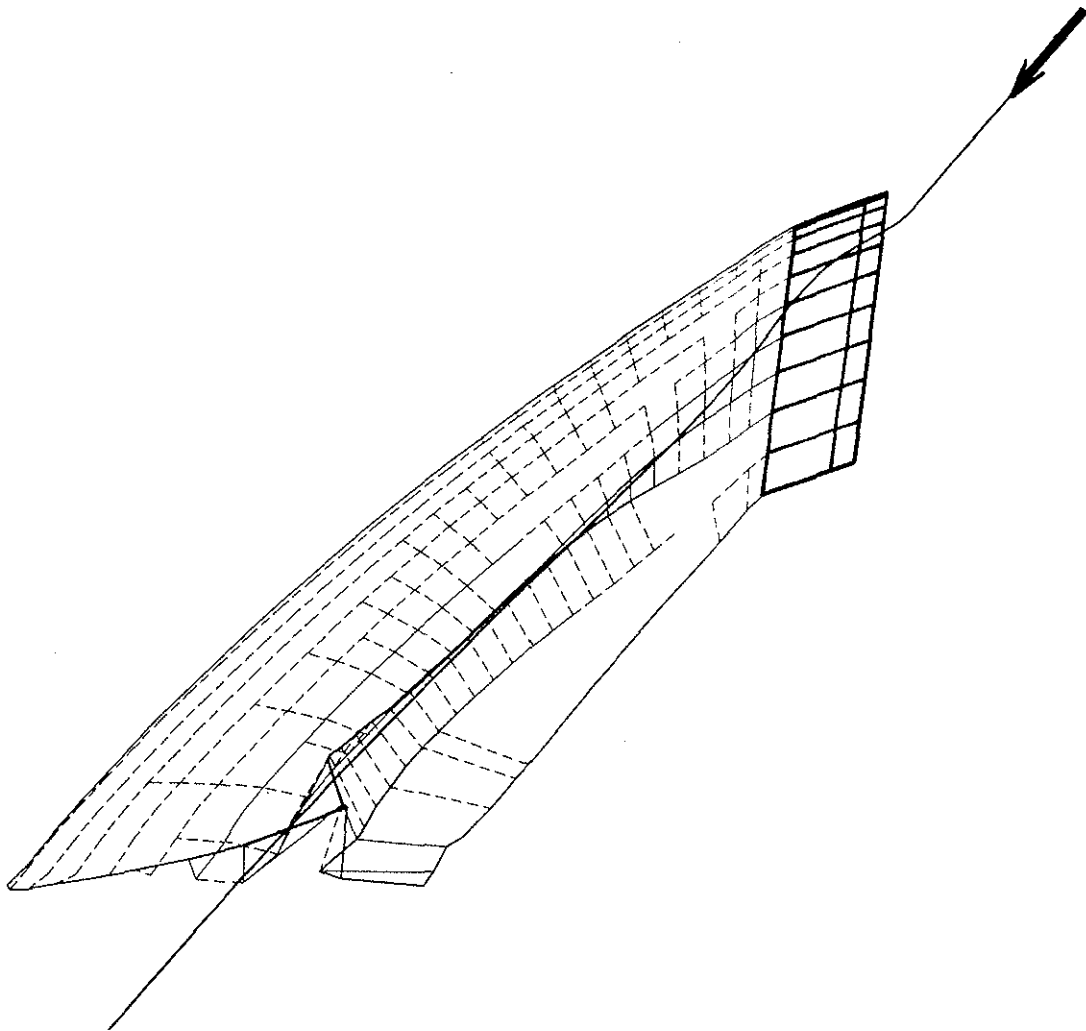
Figure 8.   Calculated wake shape at $\Psi = 150^\circ$ during a second quadrant oblique interaction where $\Gamma = 6.7 m^2/s$, $Z_v/c = 2$ and $Y_v/c = 0.2$. (Line thickness indicates vortex strength in the wake)
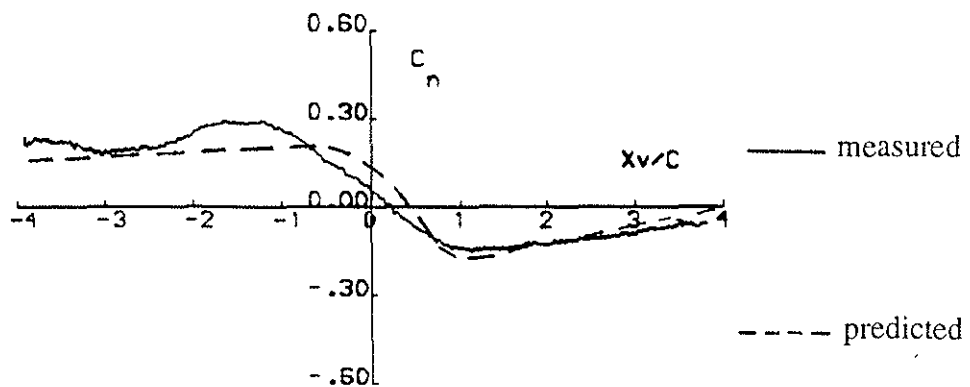
Figure 9.   Comparison of measured and predicted C_n histories during a parallel interaction with $\Gamma = 3.4 m2/s$ and $Y_v/c = 0.2$.

PIV experimental data

Wake lattice

Code simulation calculations
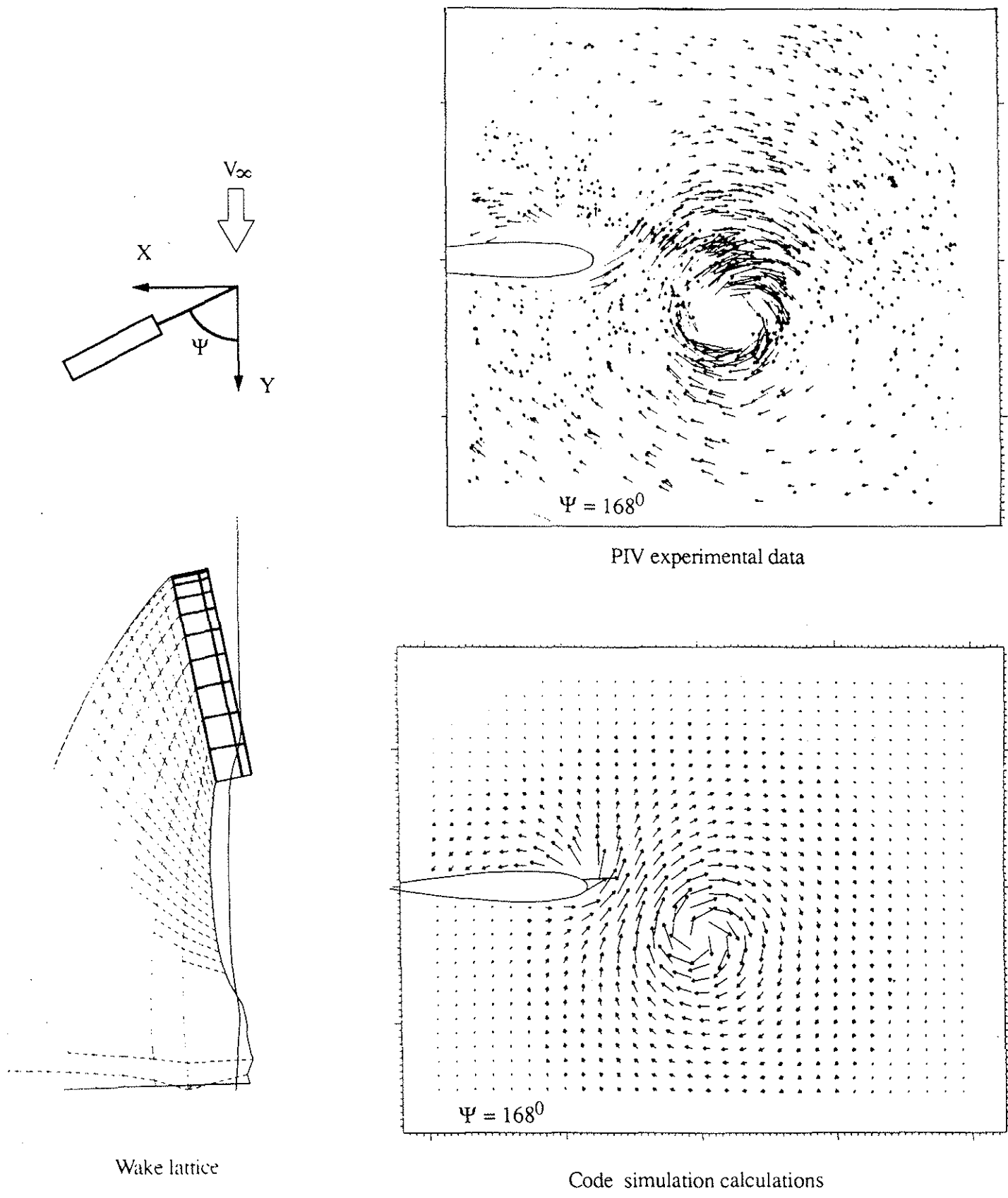
Figure 10.   Two-dimensional wake lattice, velocity map calculations with the theoretical model, and PIV velocity data at azimuth $\Psi=167.86^0$.

V_∞

X

Ψ

Y

Wake lattice

$\Psi = 176°$
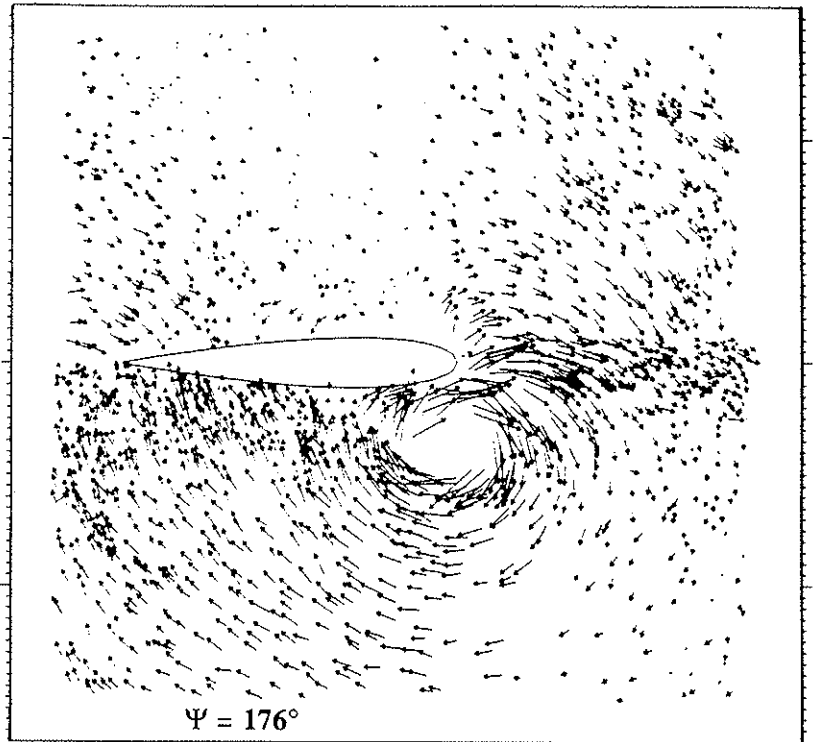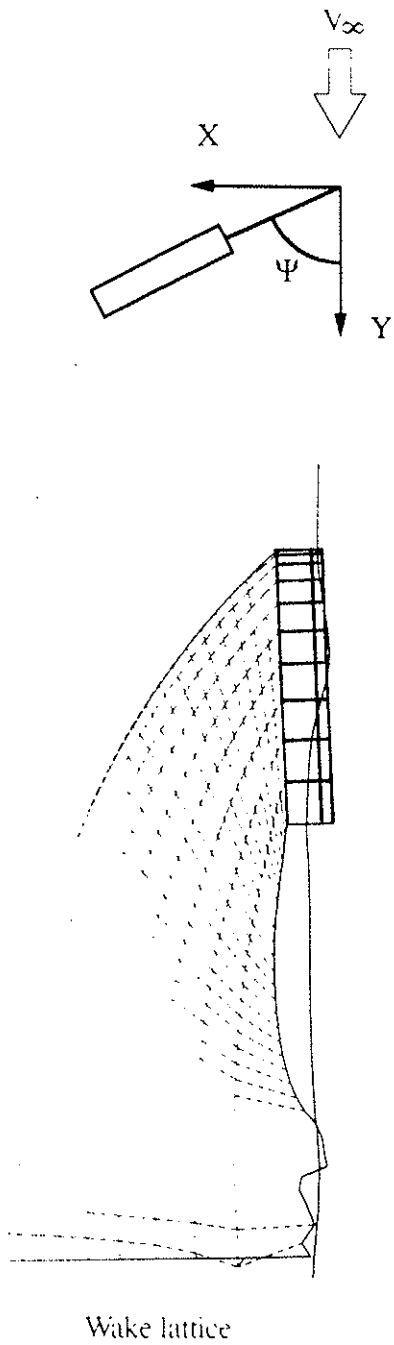
Horizontal Distance (mm)

PIV experimental data

$\Psi = 176^0$
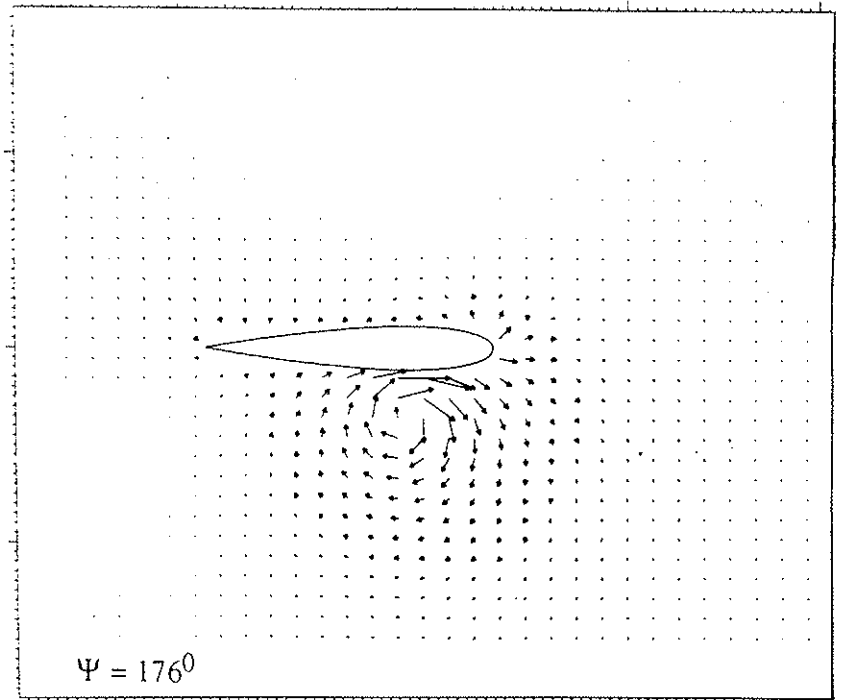
Code simulation calculations

Figure 11.   Two-dimensional wake lattice, velocity map calculations with the theoretical model, and PIV velocity data at azimuth $\Psi=176.51^0$.

V_∞

X

Ψ

Y

PIV experimental data

$\Psi = 193^0$

Wake lattice

$\Psi = 191^0$

Code simulation calculations
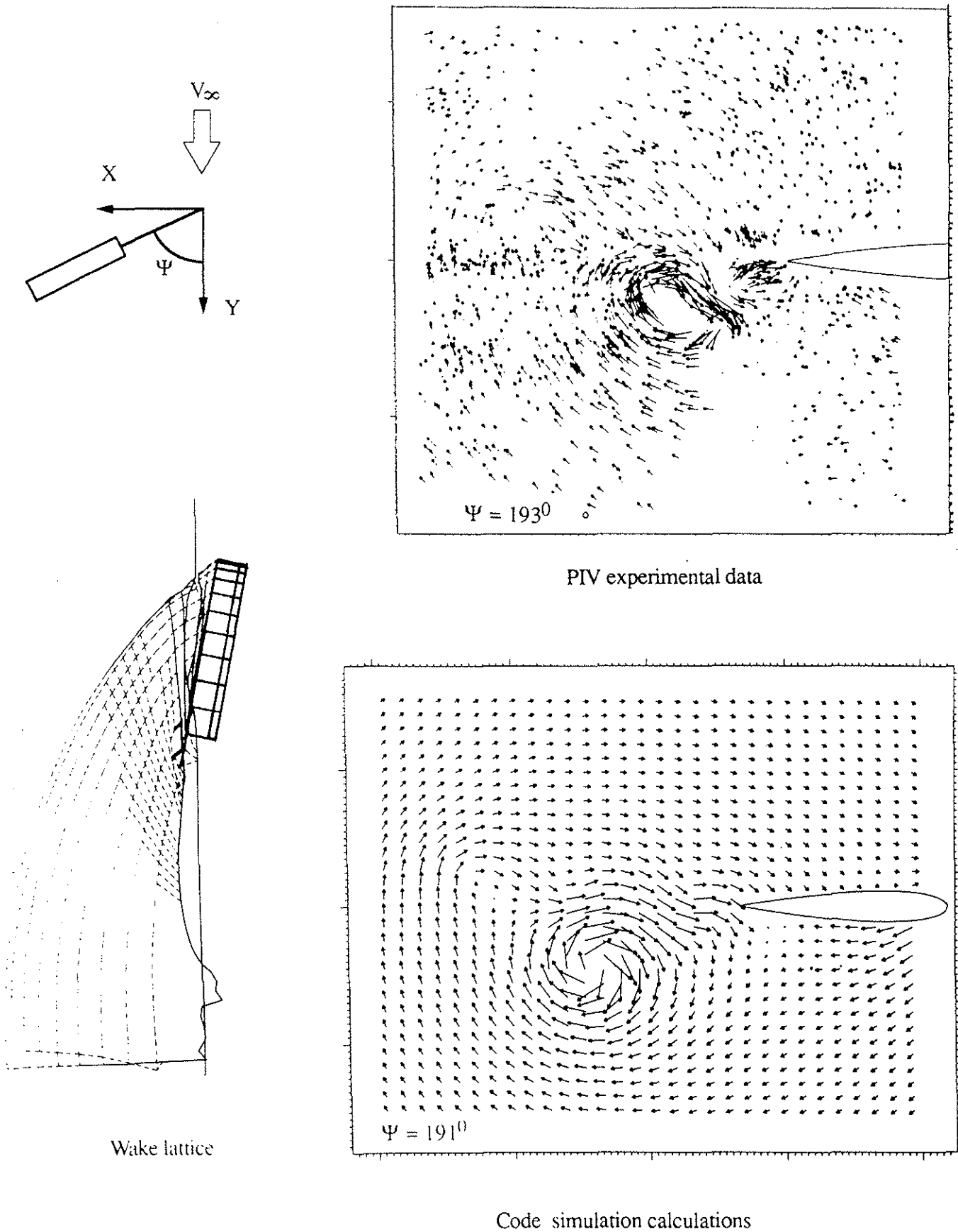
Figure 12.   Two-dimensional wake lattice, velocity map calculations with the theoretical model, and PIV velocity data at azimuth Ψ=190.93^0.